David Taylor Model Basin
Carderock Division
Naval Surface Warfare Center
9500 MacArthur Boulevard, West Bethesda, Maryland 20817-5700

NSWCCD-50-TR-2000/015 March 2000

Hydromechanics Directorate Report

A Study of Singapore Harbor-Changi Airport Wave Climatology as Determined by a New Coastal Wave Model

By
Ray Q. Lin and Andrew L. Silver

Distribution unlimited

NSWCCD-50-TR-2000/015 A Study of Singapore Harbor-Changi Airport Wave Climatology as Determined by a New Coastal Wave Model

REPORT DOCUMENTATION PAGE

Form Approved
OMB No. 0704-0188

1. AGENCY USE ONLY (Leave blank)	2. REPORT DATE	3. REPORT TYPE AND DATES COVERED
	March 2000	Final October 1999 to March 2000

4. TITLE AND SUBTITLE
A Study of Singapore Harbor-Changi Airport Wave Climatology as Determined by a New Coastal Wave Model

5. FUNDING NUMBERS
Sponsor: NFESC East Det
Order No.: WR55002
Approp.: OMN
Work Accession: DPI 5015

6. AUTHOR(S)
Ray Q. Lin and Andrew L. Silver

7. PERFORMING ORGANIZATION NAME(S) AND ADDRESS(ES)
Naval Surface Warfare Center
NSWCCD, Code 5500
9500 MacArthur Blvd.
West Bethesda, MD 20817-5700

8. PERFORMING ORGANIZATION REPORT NUMBER
NSWCCD-50-TD-2000/015

9. SPONSORING/MONITORING AGENCY NAME(S) AND ADDRESS(ES)
Naval Facilities Engineering Service Center (East Coast Detach)
1435 Pendellton Ave SE
Bldg 218, Suite 3000
Washington, DC 20374

10. SPONSORING/MONITORING AGENCY REPORT NUMBER

11. SUPPLEMENTARY NOTES

12a. DISTRIBUTION/AVAILABILITY STATEMENT
Distribution unlimited

12b. DISTRIBUTION CODE

13. ABSTRACT *(Maximum 200 words)*

A study of the wave climatology at Singapore Harbor near Changi Airport is presented to aid in determining the safety of US Navy ships in the area. Since Major wave events in Singapore Harbor mostly occur during the Northeast Monsoon season (November – March), our study focuses on this period.

In order to choose a suitable wave model to generate the climatology, a comparison of results between the State-of Art Wave Model (WAM) and the New Coastal Wave Model (NCWM) during the period of December 11, 1985 and January 13, 1986 was performed. In deep water, the difference between the results of the two models is not significant. However, in shallow water the results differ significantly. The significant wave height at Singapore Harbor calculated by the NCWM is about 3 times greater than that calculated by WAM. The buoy data agree well with the NCWM Model results. As Lin and Huang (1996b) pointed out, WAM misrepresents the coastal-trapped waves. The coastal trapped waves are highly dependent on both wave-current and wave-wave interactions.

Based on the above test, the NCWM was chosen to generate the wave climatology. The wind input and current distribution for the model are based on thirty years of data. The climatology shows that the highest and longest waves occur during the month of February

14. SUBJECT TERMS	15. NUMBER OF PAGES
Wave climatology, surface currents, tidal range, edge waves	27
	16. PRICE CODE

17. SECURITY CLASSIFICATION OF REPORT	18. SECURITY CLASSIFICATION OF THIS PAGE	19. SECURITY CLASSIFICATION OF ABSTRACT	20. LIMITATION OF ABSTRACT
UNCLASSIFIED	UNCLASSIFIED	UNCLASSIFIED	Unclassified/Unlimited

CONTENTS

FIGURES

TABLES

ABSTRACT

A study of the wave climatology at Singapore Harbor near Changi Airport is presented to aid in determining the safety of US Navy ships in the area. Since Major wave events in Singapore Harbor mostly occur during the Northeast Monsoon season (November – March), our study focuses on this period.

In order to choose a suitable wave model to generate the climatology, a comparison of results between the State-of Art Wave Model (WAM) (Komen et al, 1994)[8] and the New Coastal Wave Model (Lin and Huang, 1996a[9] and b[10]; Lin and Perrie, 1997[11] and 1999[12]) during the period of December 11, 1985 and January 13, 1986 was performed. In deep water, the difference between the results of the two models is not significant. However, in shallow water the results differ significantly. The significant wave height at Singapore Harbor calculated by the New Coastal Wave Model (NCWM) is about 3 times greater than that calculated by WAM. The buoy data agree well with the NCWM Model results. As Lin and Huang (1996b)[10] pointed out, WAM misrepresents the coastal-trapped waves. The coastal trapped waves are highly dependent on both wave-current and wave-wave interactions.

Based on the above test, the NCWM was chosen to generate the wave climatology. The wind input and current distribution for the model are based on thirty years of data. The climatology shows that the highest and longest waves occur during the month of February.

ADMINISTRATIVE INFORMATION

This study was carried out by the Seakeeping Department (Code 5500) of the Hydromechanics Directorate. The work was supported by the Naval Facilities Engineering Service Center Detachment in Washington D.C. through funding work request WR55002 and performed under Carderock Division Work Unit Number 5500-201.

1 Introduction

The US Navy requires that a wave climatology be compiled for the port of Singapore to determine the safety of its vessels there. The two critical factors needed to correctly estimate the wave climatology of Singapore Harbor are: (1) the best wave model, and (2) accurate input to model, e.g. wind, current, bottom topography.

Singapore Harbor-Changi Airport is located at $1^{o}N$ latitude and $104^{o}E$ longitude. Since it is very near the equator, the Coriolis forces ($2\Omega \sin \phi u$ and $2\Omega \sin \phi v$) are both very small, where ϕ is latitude, Ω is earth angular velocity, and u and v are the horizontal velocity in the longitude and the latitude directions, respectively. Even the rapidly changing landscapes in the area, which create large heat gradients, don't influence the generation of a steady wind field due to the small Coriolis force magnitude. As a result, the local wind waves have small amplitudes and high frequencies. The major wave events in the area occur during the monsoon seasons. Singapore Harbor has two monsoon seasons: the Southwest (May-September) and Northeast (November-March) Monsoons. During the Southwest Monsoon season, swells from the southwest-southeast aren't able to rearch Singapore Harbor because land masses restrict the wave propagation. However, during the Northeast Monsoon, swells are generated in the South China Sea, due to the continuous Northeast winds, and propagate to Singapore Harbor. Therefore, our study is focused on the Northeast Monsoon season.

Wave buoy data collected in the area, between December 11, 1985 and January 13, 1986 was available, and provided an opportunity to compare model results with observational data in shallow water.

The new coastal wave model is described in the next section, which includes the basic equations, nonlinear dispersion, and nonlinear wave-wave interactions. The input data for the model are described in Section 3. A comparison between the results of NCWM and WAM with Singapore Harbor bouy data is described in Section 4. The wave climatology

during the Northeast Monsoon at Singapre Harbor is described in Section 5.

2 A New Coastal Wave Model

2.1 Basic Equation

The basic equation for the New Coastal Wave Model is

$$\frac{\partial \mathbf{A}}{\partial t} + \frac{\partial [c_{g\lambda}\mathbf{A}]}{\partial \lambda} + \cos\phi^{-1}\frac{\partial [c_{g\phi}\cos\phi\mathbf{A}]}{\partial \phi} + \frac{\partial [c_{\theta}\mathbf{A}]}{\partial \theta} + \frac{\partial [c_{\omega}\mathbf{A}]}{\partial \omega} = S_{in} + S_{ds} + S_{nl}, \quad (1)$$

in which $\mathbf{A}$ $(m^2/Hz^2/radians)$ is the action density spectrum defined as the energy spectrum divided by the intrinsic frequency σ, a generalized definition of action for a single train of waves (Bretherton and Garrett, 1968[1], and i Günther et al., 1993[2]); t is the time (s); ϕ and λ are the latitude and longitude coordinates respectively; θ is the propagation angle (when θ equals 0, the direction is from the south, with the direction orientation rotating clockwise as θ increases); and S_{in} is the wind input function (Janssen, 1991[6]), S_{ds} is the dissipation, wave-breaking, term (Komen et al, 1994[8]), and S_{nl} is the nonlinear wave-wave interaction term (Lin and Perrie, 1999[12]).

Equation (1) differs from the one used in the WAM. The WAMDI Group (1988)[15] used an equation for the conservation of energy in a form similar to Equation (1), but it was designated as 'the transport equation' in intrinsic frequency space by assuming steady water depth and current, i.e.

$$\frac{\mathbf{DN}}{\mathbf{Dt}} = \frac{\partial \mathbf{N}}{\partial t} + \frac{\partial (c_{g\lambda}+u)\mathbf{N}}{\partial \lambda} + \cos\phi^{-1}\frac{\partial (c_{g\phi}+v)\mathbf{N}}{\partial \phi} + +\sigma\frac{\partial (c_{\sigma}\frac{\mathbf{N}}{\sigma})}{\partial \sigma} + \frac{\partial c_{\theta}\mathbf{N}}{\partial \theta} = S_{in}+S_{ds}+S*_{nl}, \quad (2)$$

in which $\mathbf{N}$ $(m^2/Hz/radians)$ is the energy density spectrum. S^*_{nl} is based on the Discrete Integration Approximation, (DIA) by Hasselman and Hasselmann[3].

To consider the implications of topography, finite depth, time-dependent currents and nonlinear dispersion, we must consider the characteristic propagation velocities c_{θ}, c_{ω}, $c_{g\lambda}$,

and $c_{g\phi}$. A full discussion of these terms is given by Lin and Huang (1996b)[10] and Lin (1998)[13]. The group velocities in the longitudinal and latitudinal directions, $c_{g\lambda}$ and $c_{g\phi}$ may be represented as:

$$c_{g\lambda} = \frac{D\lambda}{Dt} = \frac{c_g \sin\theta + u}{R\cos\phi}, \tag{3}$$

$$c_{g\phi} = \frac{D\phi}{Dt} = \frac{c_g \cos\theta + v}{R}, \tag{4}$$

where R is the earth's radius. These expressions are found in both the NCWM and the WAM, as well as other standard modern wave models. Formulations for $c_\theta = \frac{D\theta}{Dt}$ and $c_\omega = \frac{D\omega}{Dt}$ are

$$c_\theta = \frac{1}{k}\frac{\partial\sigma}{\partial d}\frac{\partial d}{\partial n} + \frac{1}{k}(c_g - c)\frac{\partial k}{\partial n} + \frac{\vec{k}}{k}\cdot\frac{\partial\vec{V}}{\partial n}; \tag{5}$$

$$c_\omega = \frac{D\omega}{Dt} = \frac{\partial(\sigma + \vec{k}\cdot\vec{V})}{\partial t} + (\vec{c}_g + \vec{V})\cdot\nabla(\sigma + \vec{k}\cdot\vec{V}), \tag{6}$$

where $\vec{0}$ is vector, following the nonlinear dispersion in Equation (9) below, and also in Lin and Huang (1996b)[10]. These are implemented in NWCM.

These c_θ and c_ω expressions differ significantly from those implemented in standard linear dispersion wave models such as the WAM or Tolman (1991[16], 1992[17]). In the former case, c_θ and c_ω are given by:

$$c_\theta = \frac{1}{k}\frac{\partial\sigma}{\partial d}\frac{\partial d}{\partial n} + \frac{\vec{k}}{k}\cdot\frac{\partial\vec{V}}{\partial n}; \tag{7}$$

$$c_\omega = 0. \tag{8}$$

2.2 The Dispersion Relationship Used in the NCWM

Although the effects of nonlinearities are usually small in wave propagation (Lin and Huang, 1996a[9]), the need for a full nonlinear dispersion relation has been made amply clear by nu-

merous papers on nonlinear wave evolution (see, for example, Yuen and Lake, 1982[19]; Infeld and Rowlands[5], 1990). The nonlinear dispersion relationship is not only a factor governing the modulation and propagation of the waves, but also a key in modifying the resonant interaction conditions as reported by McLean (1982)[14]. Therefore, it is not only logically imperative but also intellectually satisfying to adopt such a fuller dispersion relationship. For these reasons, we decided to adopt the full nonlinear dispersion as given in Whitham (1974)[18] and examine its effects. Following Whitham, we have

$$\sigma = \left\{(gk\tanh kd)[1 + (\frac{9\tanh^4 kd - 10\tanh^2 kd + 9}{8\tanh^4 kd})k^2a^2 + ...]\right\}^{1/2}, \tag{9}$$

in which σ is the intrinsic frequency in $radian/s$; k is the magnitude of the vector wave number, $\vec{k}$, in m^{-1}; g is gravitational acceleration (m/s^2); d is the depth (m), and a is the amplitude of the wave.

By definition,

$$\vec{c}_g = \frac{\partial\sigma}{\partial k}\frac{\vec{k}}{k}, \qquad \vec{C} = \frac{\omega}{k}\frac{\vec{k}}{k}, \qquad and \qquad \vec{c} = \frac{\sigma}{k}\cdot\frac{\vec{k}}{k}, \tag{10}$$

where $\vec{c}_g$ is the intrinsic group velocity; ω is the apparent frequency defined as $\omega = \sigma + \vec{k}\cdot\vec{V}$ with $\vec{V}$ as the ambient current in m/s; $\vec{C}$ and $\vec{c}$ are the apparent and intrinsic phase velocities respectively. In terms of the spectral representation, the full nonlinear group velocity should be

$$\begin{aligned}\vec{c}_g = &\left\{0.5[\frac{g}{k}\tanh kd]^{1/2}[1 + \frac{2kd}{\sinh(2kd)}][1 + f_{p(k,d)}k^2\hat{\mathbf{N}}]^{1/2}\right\}\frac{\vec{k}}{k} \\ &+ \left\{0.5\frac{(gk\tanh kd)^{1/2}}{[1 + f_{p(k,d)}k^2\hat{\mathbf{N}}]^{1/2}}[(\frac{\partial\hat{\mathbf{N}}}{\partial k}k^2 + 2k\hat{\mathbf{N}})f_{p(k,d)} + k^2d\hat{\mathbf{N}}df_{p(k,d)}]\right\}\frac{\vec{k}}{k},\end{aligned} \tag{11}$$

in which $\hat{\mathbf{N}}$ is total energy spectrum, and $f_{p(k,d)}$ and $df_{p(k,d)}$ are given as follows:

$$f_{p(k,d)} = \frac{9}{8} - \frac{10}{8\tanh^2 kd} + \frac{9}{8\tanh^4 kd}, \tag{12}$$

$$df_{p(k,d)} = \frac{10sech^2kd}{4\tanh^3 kd} - \frac{9sech^2kd}{2\tanh^5 kd}. \tag{13}$$

It should be noted that when we consider the presence of time varying tidal currents, not only a, but also d are functions of position and time. With the introduction of the position-dependent amplitude and depth in the nonlinear dispersion relationship, the wave number can no longer be assumed to be conserved automatically. Rather, we should have

$$\sigma = W[k(x,t), d(x,t), a(x,t)]; \tag{14}$$

therefore, following the group velocity, we have

$$\frac{Dk_i}{Dt} = -\frac{\partial W}{\partial d}\frac{\partial d}{\partial x_i} - \frac{\partial W}{\partial a}\frac{\partial a}{\partial x_i}, \tag{15}$$

with $\frac{D()}{Dt}$ the material derivative following the wave group. Here, we have considered variations of both the amplitude and the depth and assumed that they are of the same order of magnitude. These variations of wave number and frequency have been neglected by all previous modelers, but they have been clearly pointed out as important considerations in the nonlinear wave evolution process by Whitham (1974)[18], in a discussion of wave kinematics. They should thus be included in the coastal wave model.

2.3 Nonlinear Source Function

Wave-wave interactions cause energy density spectrum frequency downshifting and play a major role in wave growth. In shallow water, wave-wave interactions increase rapidly as depth decreases. It is important to correctly calculate the nonlinear source function.

The Discrete Integration Approximation method (DIA)[3] is a parameterization method for calculating nonlinear wave-wave interactions in deep water. In shallow water, due to the rapidly increasing nonlinearity with decreasing depth, the nonlinear wave-wave interactions not only become far more important than those in the deep ocean but also become far more complicated. In the deep ocean the four equivalent gravity wave interactions dominate.

However, in shallow water, these interactions do not always dominate. The interactions between gravity waves and swells, the interactions between the gravity waves and the bottom topographic wave or the edge waves, etc. may become more important. Parameterization methods represent such complicated phenomenon with great difficulty. Therefore, it becomes necessary to use an 'exact method' to calculate the wave-wave interactions. Hasselmann and Hasselmann[4] first presented their 'exact solution' for a wide range of wave spectra. However, their method uses too much CPU time, making it impractical. Resio and Perrie (1991) reduced the classical method[4] from five-dimensional integrations to three-dimensional integrations by integrating along the resonant orbit. Lin and Perrie (1999[12]) reduced the three-dimensional integrations to quasi-line integrations, (the reduced interaction approximation, RIA), based on highly nonlinearly distributed coefficients. In 1998, Base Enhancement Wave Prediction Conference (an international competition) (Jensen et al., 1998[7]) showed that these three 'exact solution' methods obtain similar results for wide range of spectra, as well as for a split wave spectrum, when $kd \geq 0.7$, and the dispersion is linear. However, the RIA method is about 3-orders of magnitude faster than the method of Hasselmann and Hasselmann[4], and 2-orders of magnitude faster than that of Resio and Perrie. Furthermore, the RIA method allows $kd \geq 0.3$ instead of $kd \geq 0.7$, and $ka \leq 0.3$ instead of $ka \leq 0.06$, values much more suitable for shallow water. The details of the RIA method can be found in Lin and Perrie (1997[11] and 1999[12]).

3 Model Input Functions

In order to compile an accurate wave climatology for the Northeast Monsoon in Singapore Harbor, we first need to accurately predict the waves generated in the South China Sea. Swell develops in that area and propagates to Singapore Harbor. Secondly, details of the local environment of Singapore Harbor must be known, in order to understand how the swell

propagates to the Harbor as well as how the swell interacts with the local waves and currents. For the above reasons, the simulation domain includes the area from 5^oS to 20^oN latitude and from 99^oE to 120^oE longitude. The input data for the wave model are:

1) The bottom topography as shown in Fig. 1. The water depths just offshore are very deep, so it is assumed that no edge waves are present;

2) The monthly wind data (mean, maximum and extreme maximum), was obtained from 30 years of wind data at 3 stations: a). 22^oN, 103^oE; b) 12^oN, 106^oE; c) 1^oN and 104^oE, as shown in Table 1. Then the whole simulation domain was linearly interpolated.

3) The seasonal current data was simply adopted from the Fleet Numerical Oceanographic Center in Asheville, North Carolina for the South China Sea and extend to Singapore Harbor, using the local data as shown in Fig. 2;

4) The dominant semi-diurnal tidal current. The amplitude of the tidal current is 0.4m/s, and water depth varies by about 2.3 meters.

4 Model Results

According to thirty-year correlations between the local wind data at Singapore Harbor and the other two stations (22^oN, 103^oE; and 12^oN, 106^oE), we generated wind data for these two stations during December 11, 1985-January 13, 1986. The Table 2 shows wind data of Singapore Harbor, and these two stations during 12/11/85-1/13/86. Based on Table 2, we generated the wind input over the whole computational domin.

Table 3a shows the predicted waves from WAM and NCWM at 15^oN and 114^oE from December 11, 1985 to January 13, 1986. The water depth at this location is greater than 1000 meters. From Table 3a, we can see that results of the two models do not differ significantly. The maximum difference between the two models, in the significant wave height, is about 25%.

However, the model results between WAM and NCWM are entirely different in shallow water, such as Singapore Harbor, where the water depth is about 30 meters. Table 3b shows the model results and observational buoy data collected during this period at $1^{o}N$, and $104^{o}E$. The results of the NCWM agree well with the buoy data in significant wave height, wave period, as well as maximum wave height and maximum wave period. However, for WAM, the significant wave height is about one third of the buoy data and the wave period is 0.6 times of buoy data. This may due to the fact that WAM doesn't include tidal currents and the water depths varying with time (Section 2.1), nonlinear dispersion (Section 2.2), or the swell interactioning with local waves (Section 2.3), etc. Coastal trapped waves do not appear at Singapore Harbor in WAM, but they do appear in NCWM results.

5 The Singapore Harbor Wave Climatology

Table 4 shows a summary of the Singapore Harbor wave climatology, during the Northeast Monsoon, by the as predicted by the NCWM model. Thus, we conclude that the greatest significant wave height and the longest period wave occurs in February. The smallest occurs in November.

Fig. 3 shows one dimensional monthly mean energy density spectrum for the past 30 years. The semi-diurnal period is presented. Each figure represents a one-hour mean spectrum. The maximum variations during the semi-diurnal tidal current are 0.016 (Nov.), 0.02 (Dec.), 0.026 (Jan.), 0.042 (Feb.), and 0.016 (Mar.), unit is meter).

Fig. 4 is the same as Fig. 3, except that it shows the one-dimensional monthly maximum energy density spectrum. This maximum energy density spectrum represents the maximum monthly wind during the past 30 years. The maximum variations during the semi-diurnal tidal current are 0.16 (Nov.), 0.21 (Dec.), 0.26 (Jan.), 0.34 (Feb.), and 0.23 (Mar.), unit is meter.

Finally, Fig. 5 shows a one dimensional extreme maximum energy density spectrum, which is based on the daily maximum wind occurring at the full tidal current in the year which had the maximum wind in the last 30 years. It represents the extreme maximum limit of the spectral cases.

6 Summary

Based on our comparisons, we conclude that NCWM will produce more realistic results than WAM due to improved numerics, new kinematics, and a new nonlinear source function. From the model results, we can see that there are significant differences between WAM and NCWM when there is a steady or unsteady current, or a rough bottom topography and shallow water.

Therefore, in this study, we use NCWM to study the wave climatology. Singapore Harbor is located at $1^{o}N$ and $104^{o}E$. The Coriolis force is extremely small. Local wind gusts wind may occur due to the uneven heating of the landscape. However, without the Coriolis force, the heat gradients balance very quickly. Except during the monsoon seasons, local waves are very small in amplitude and very high in frequency. During the Southwest Monsoon season, the swell from the south can't reach Singapore Harbor due to the surrounding land. During the Northeast Monsoon season, swell generated in the South China Sea can reach Singapore Harbor. Therefore, in this study, we focused on the Northeast Monsoon season. During this season, the extreme wave cases usually occur in February. The smallest occur in November.

Acknowledgements

We would like to thank William Seeling of Naval Facilities Engineering Service Center East Coast Detachment for sponsoring this project. We also thank Brian Wallace for providing useful current and wind data in the South China Sea during the Northeast Monsoon season.

References

[1] Bretherton, F. P. and C. J. R. Garrett, Wave trains in inhomogeneous moving media. Proc. Roy. Soc. London, A302, 529-554, (1968)

[2] Günther, H., Hasselmann, S., P.A.E.M. Janssen, The WAM model cycle4. DKRZ WAM Model Documentation, (1993)

[3] Hasselman, S. and K. Hassleman, A symmetrical method of computing the nonlinear transfer in a gravity-wave spectrum, Hamb. Geophys. Einzelschriften Reihe A Wiss. Abhand., 52, 138pp, (1981).

[4] Hasselmann, S. and K. Hasselmann, Computation and parameterization of the nonlinear energy transfer in a gravity-wave spectrum. Part I: A new method for efficient computations of exact nonlinear transfer integral. J. of Phys. Oceanogr. Vol. 15, 1369-1377, (1985).

[5] Infeld, E. and G. Rowlands, Nonlinear Waves, Solitons and Chaos, Cambridge University Press, 423pp, (1990).

[6] Janssen, P.A.E.M., Quasi-linear theory of wind wave generation applied to wave forecasting. J. of Phys. Oceanogr.,, Vol. 21, 1631-1642.

[7] Jensen, R., D. Resio, R.-Q. Lin, G. Van Vledder, T. Harber, and B. Tracy, A report of competition of nonlinear source function in Base Enhancement Wave Prediction Conference, (1998).

[8] Komen, G. J. L., Cavaleri, M. Donelan, K. Hasselmann, and P. A. E. M. Janssen, Dynamics and Modelling of Ocean Waves. Cambridge University Press. 532pp, (1994).

[9] Lin, R. Q. and N. E. Huang, The Goddard Coastal Wave Model. Part I. Numerical Method. J. Phys. Oceanogr., Vol. 26, No. 6, 833-847, (1996a).

[10] Lin, R. Q. and N. E. Huang, The Goddard Coastal Wave Model. Part II. Kinematics. J. Phys. Oceanogr., Vol. 26, No. 6, 848-862, (1996b).

[11] Lin, R. Q. and W. Perrie, A New Coastal Wave Model. Part III. Nonlinear Wave-wave Interactions. J. Phys. Oceanogr., Vol. 27, No. 9, 1813-1826, (1997).

[12] Lin, R. Q. and W. Perrie, Wave-wave Interaction in Finite Depth Water. J. Geophy. Res., Vol. 104, No. C5, 11193-11213, (1999).

[13] Lin, R. Q., Reply. J. Phys. Oceanogr.,, Vol. 28, 1309-1318, (1998).

[14] McLean J. W., Instabilities of finite-amplitude gravity waves on water of finite depth. J. of Fluid Mech., 114, 331-341, (1982).

[15] The WAMDI Group, The WAM model-a third generation ocean wave prediction mode.J. Phys. Oceanogr., 18, 1775-1810, (1988).

[16] Tolman, H. L., A third-generation model for wind waves on slowly varying, unsteady, and inhomogeneous depth and currents. J. of Phys. Oceanogr., Vol. 21, 782-797, 1991.

[17] Tolman, H. L., Effects of numerics on the physics in a third-generation wind-wave model. J. of Phys. Oceanogr., Vol. 22, 1095-1111, 1992.

[18] Whitham, G. B., Linear and Nonlinear Waves. John Wiley, New York, 636pp, (1974).

[19] Yuen, H. C. and B. M. Lake, Nonlinear dynamics of deep-water gravity waves. Adv. Appl. Mech., 22, 69-229, (1982).

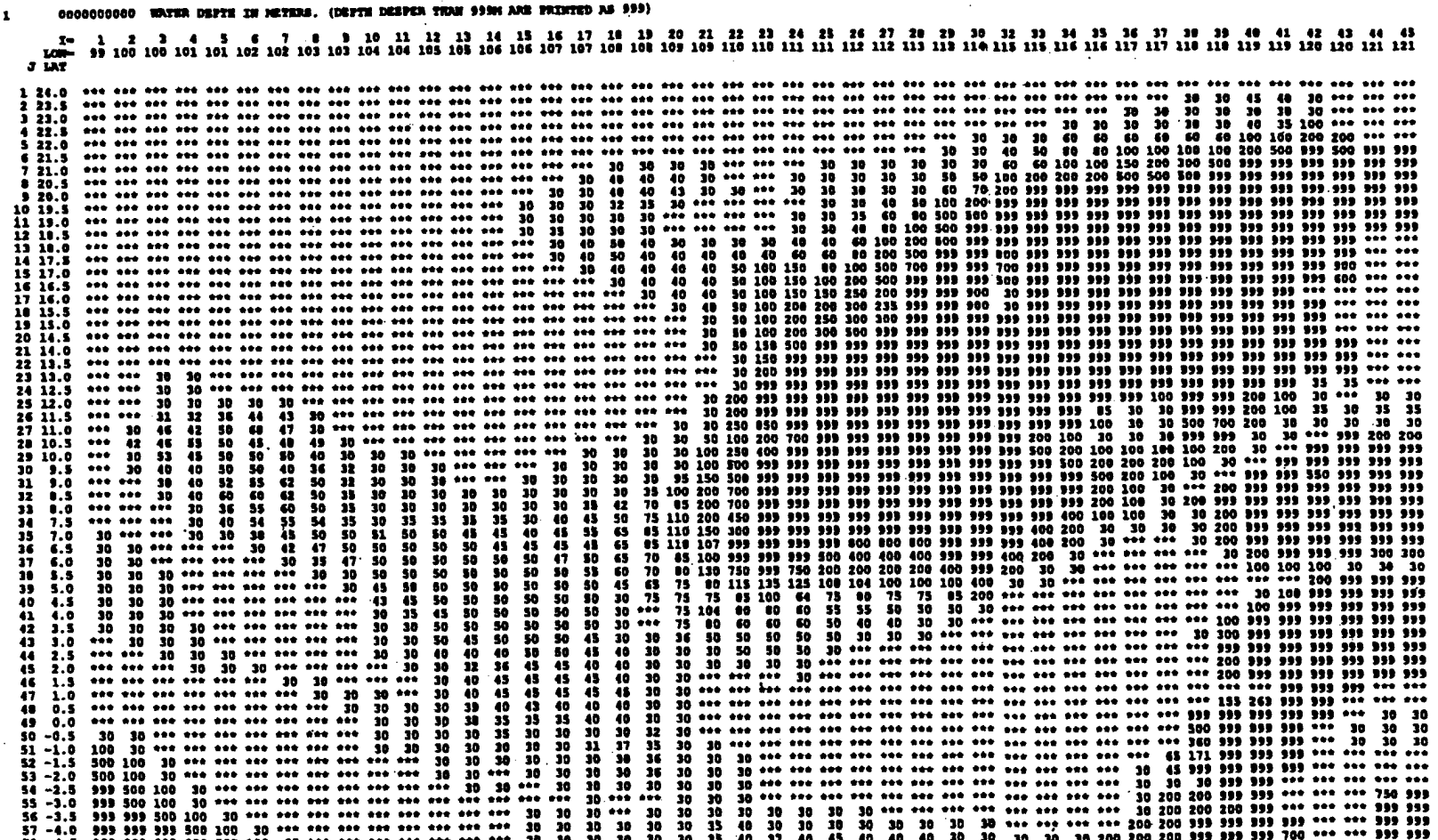

Fig. 1. The bottom topography from $5°S$ to $20°N$ latitude and $99°E$ to $120°E$.

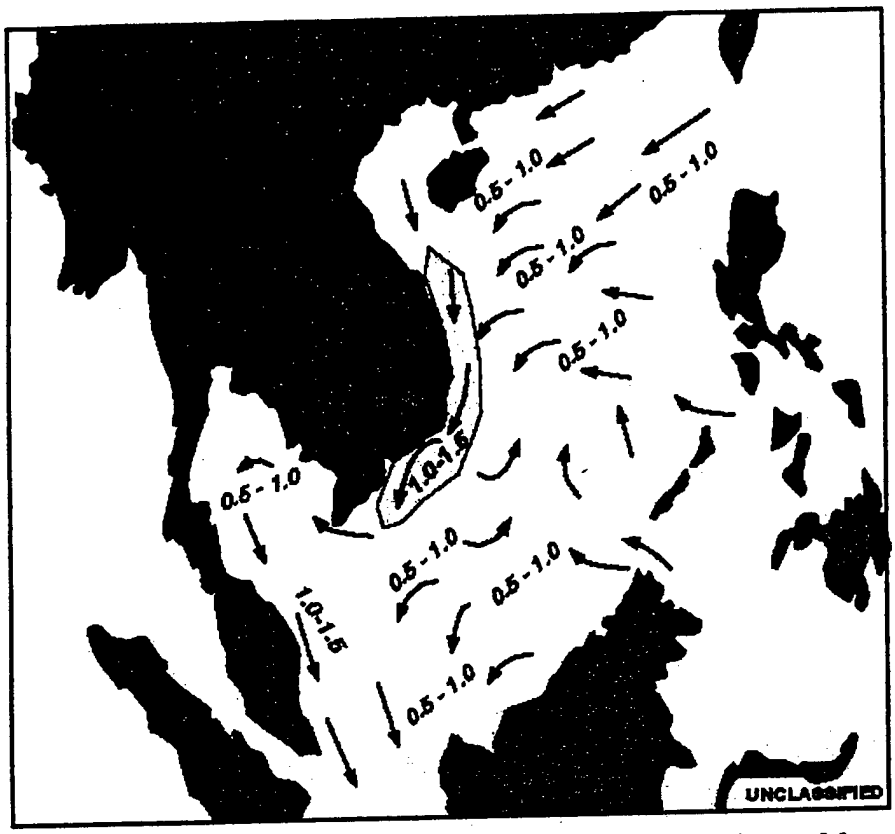

Fig. 2. The seasonal mean current during the Northeast Monsoon season associated with the area shown in Fig. 1.

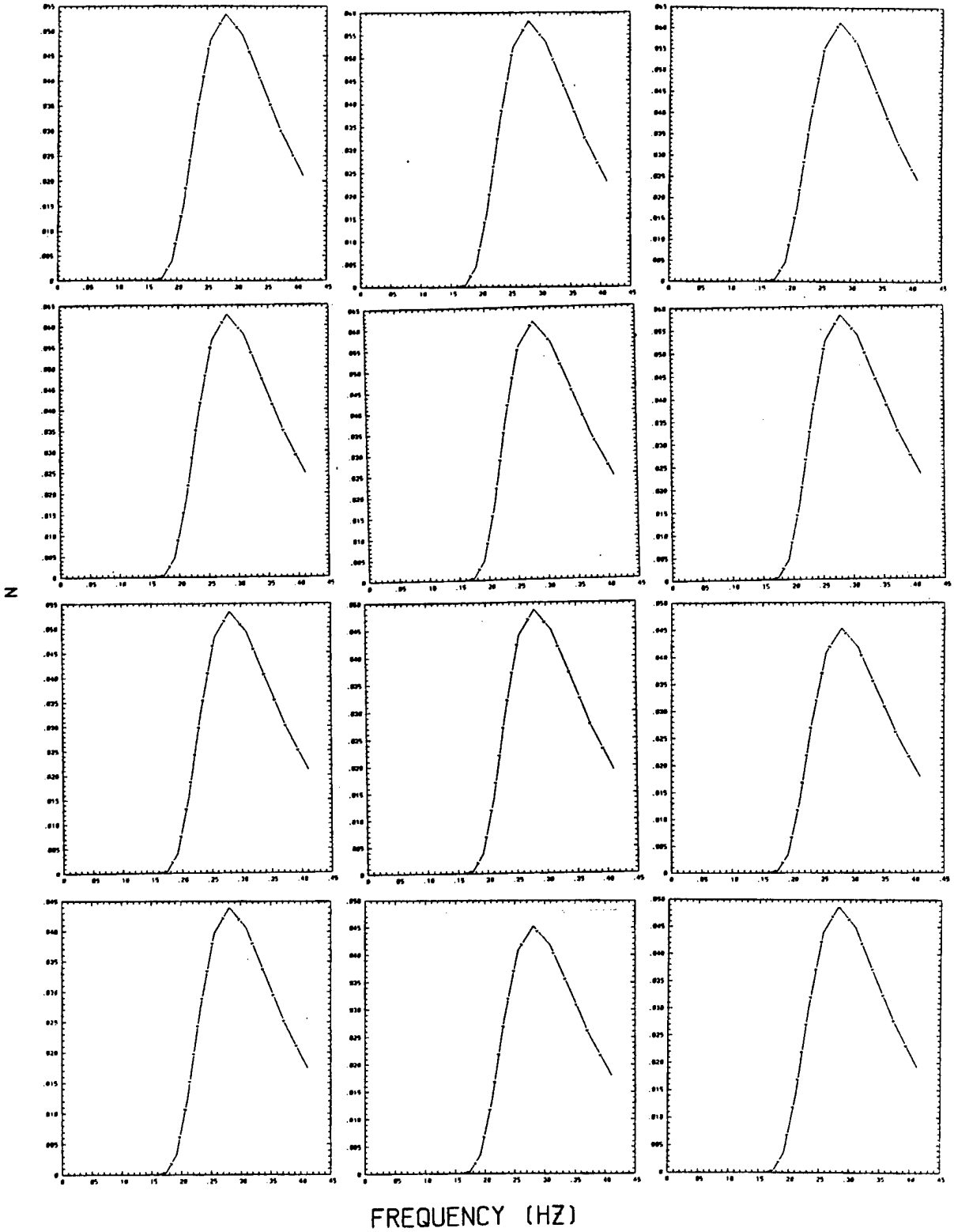

Fig. 3a. November energy density spectrum.

Fig. 3. One-dimensional monthly mean spectrum during the past 30 years. The semi-diurnal tidal current dominates in this area, each figure represents a hour mean spectrum.

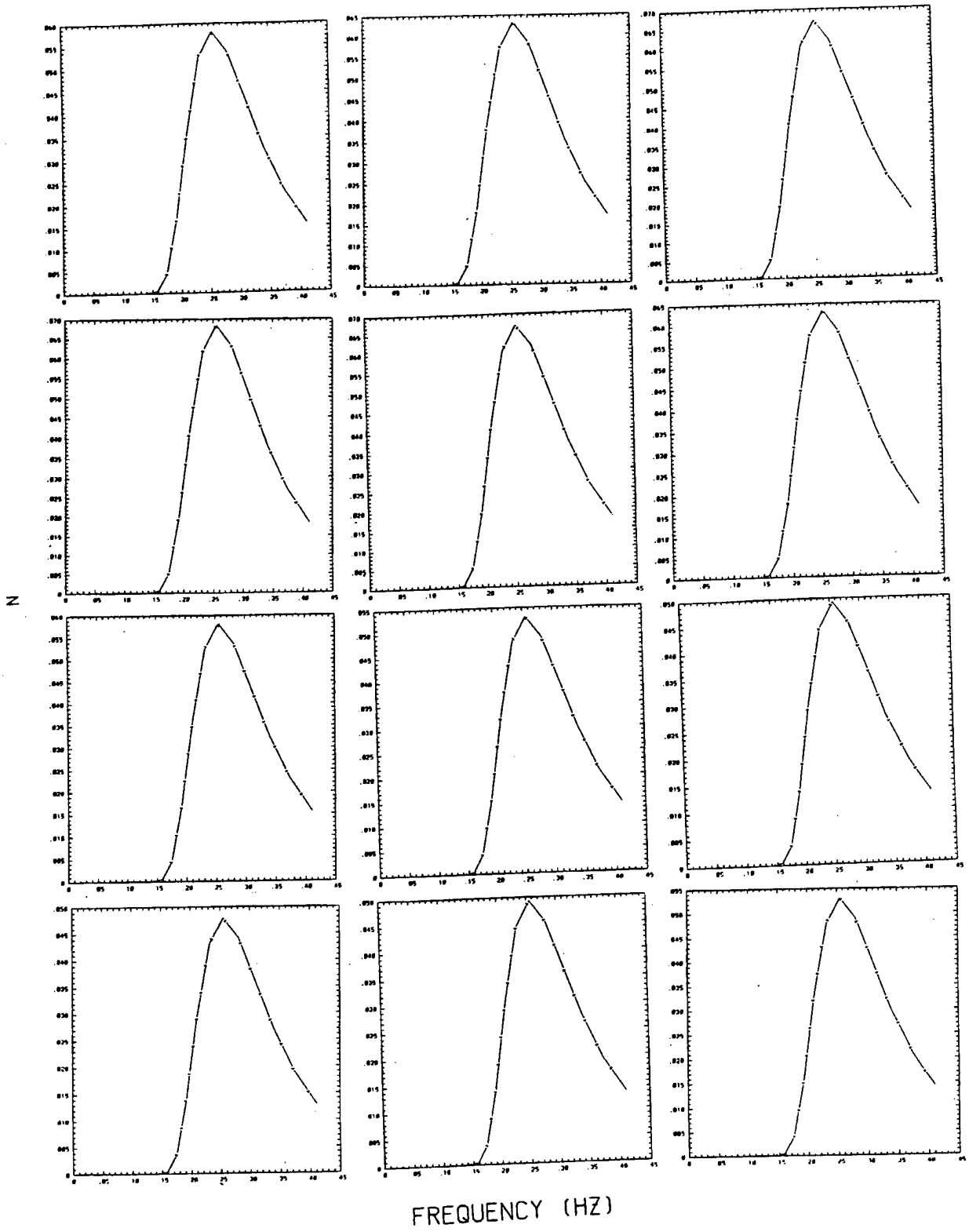

Fig. 3b. December energy density spectrum.

Fig. 3. (Continued)

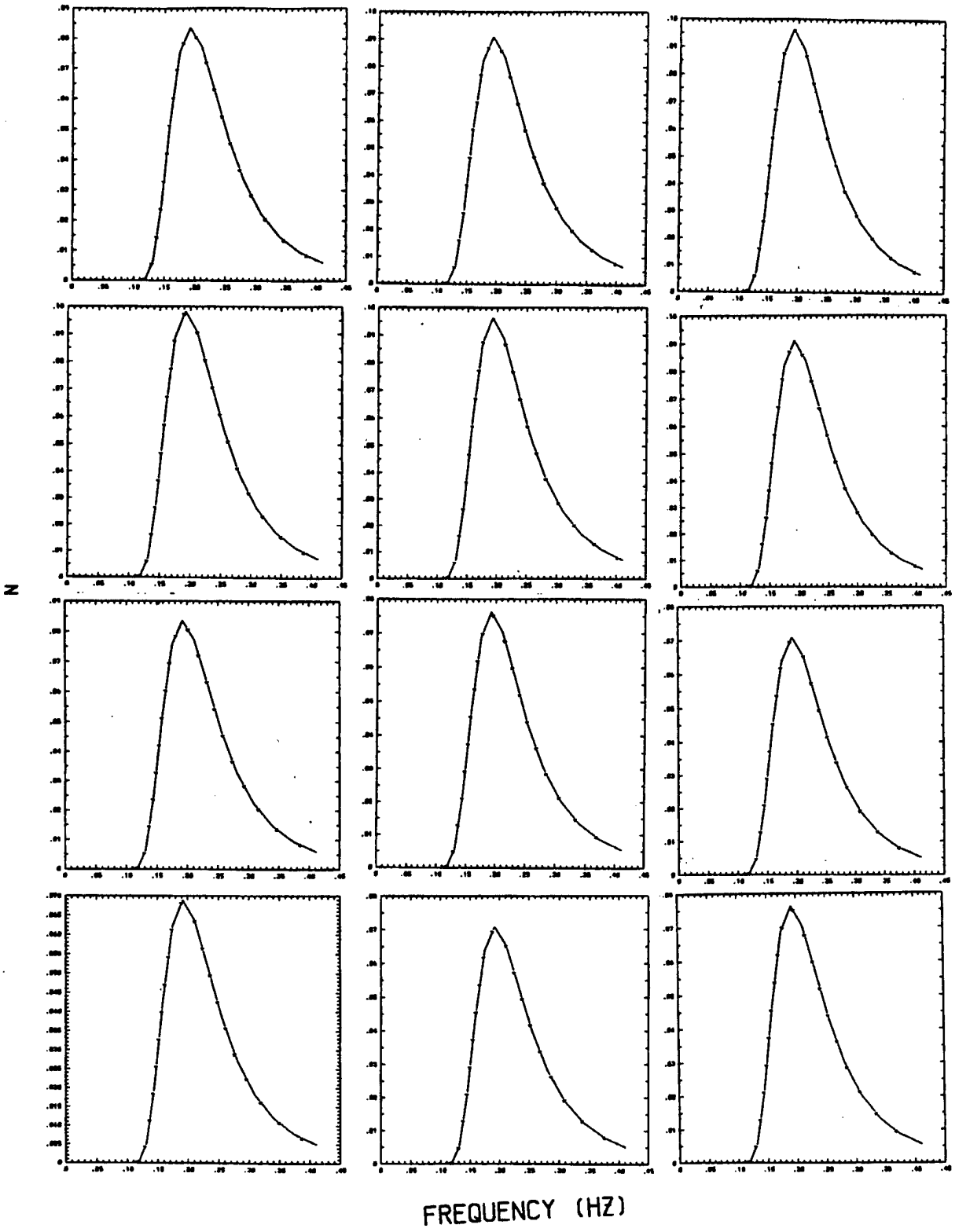

Fig. 3c. January energy density spectrum.

Fig. 3. (Continued)

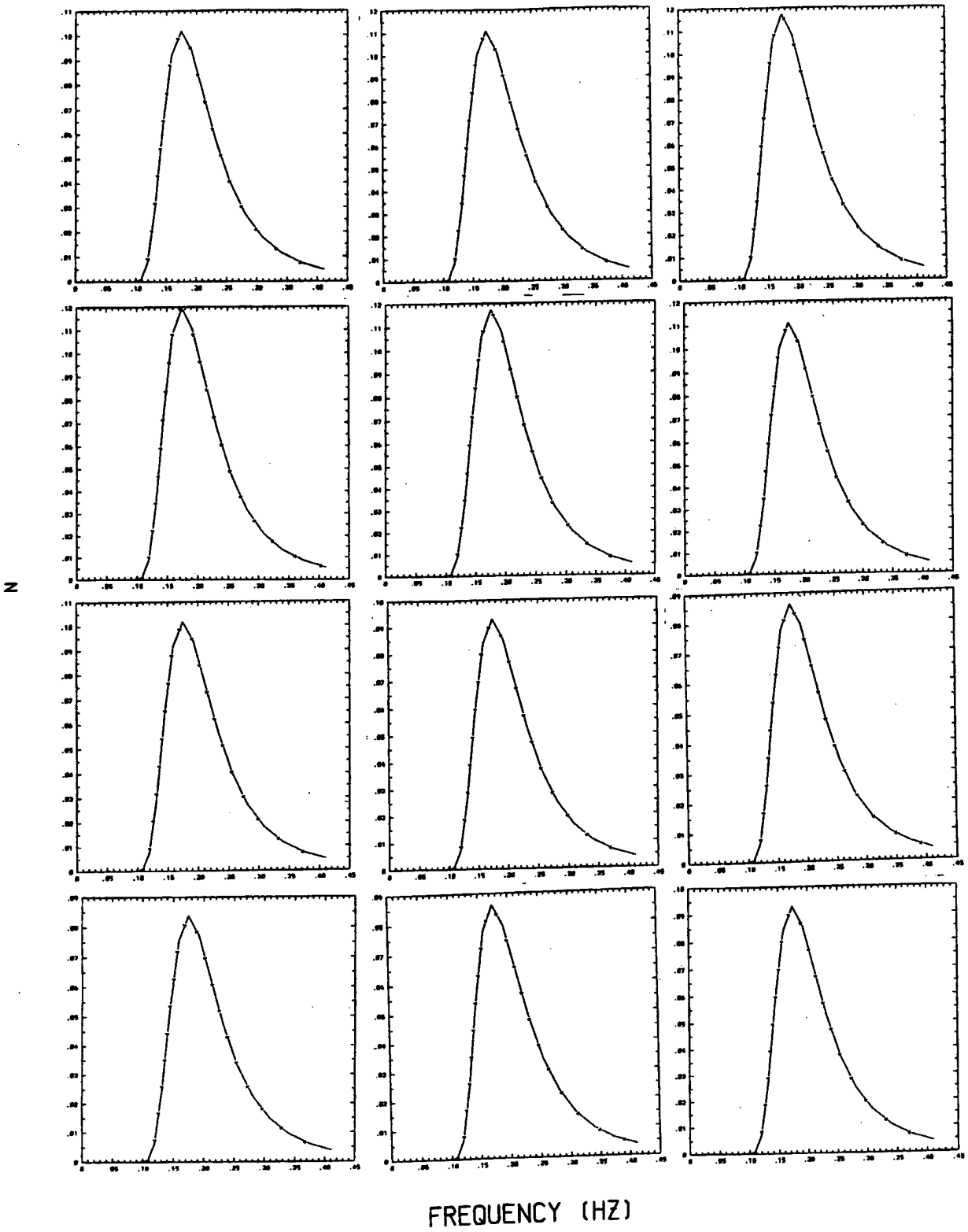

Fig. 3d. February energy density spectrum.

Fig. 3. (Continued).

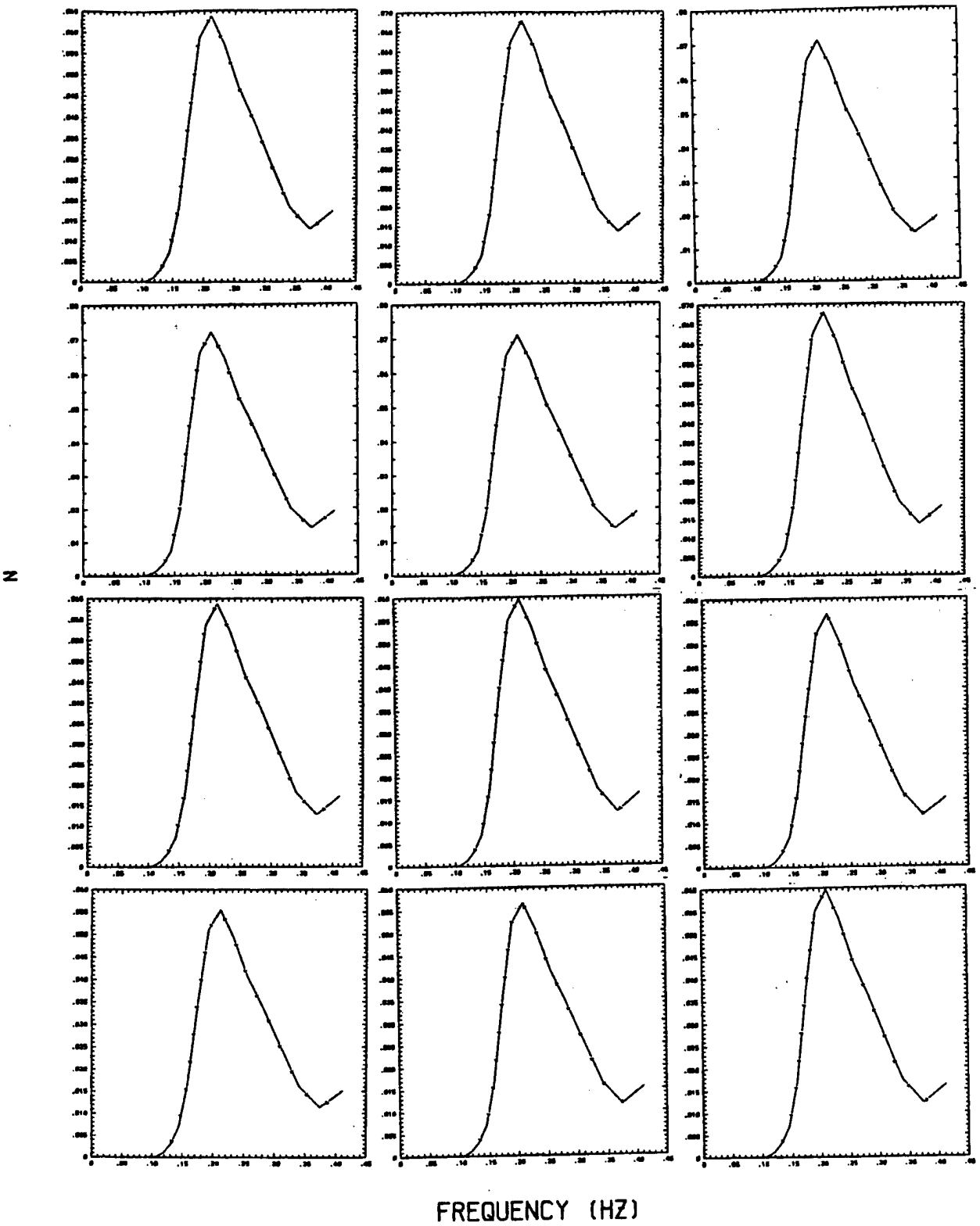

Fig. 3e. March energy density spectrum.

Fig. 3. (continued)

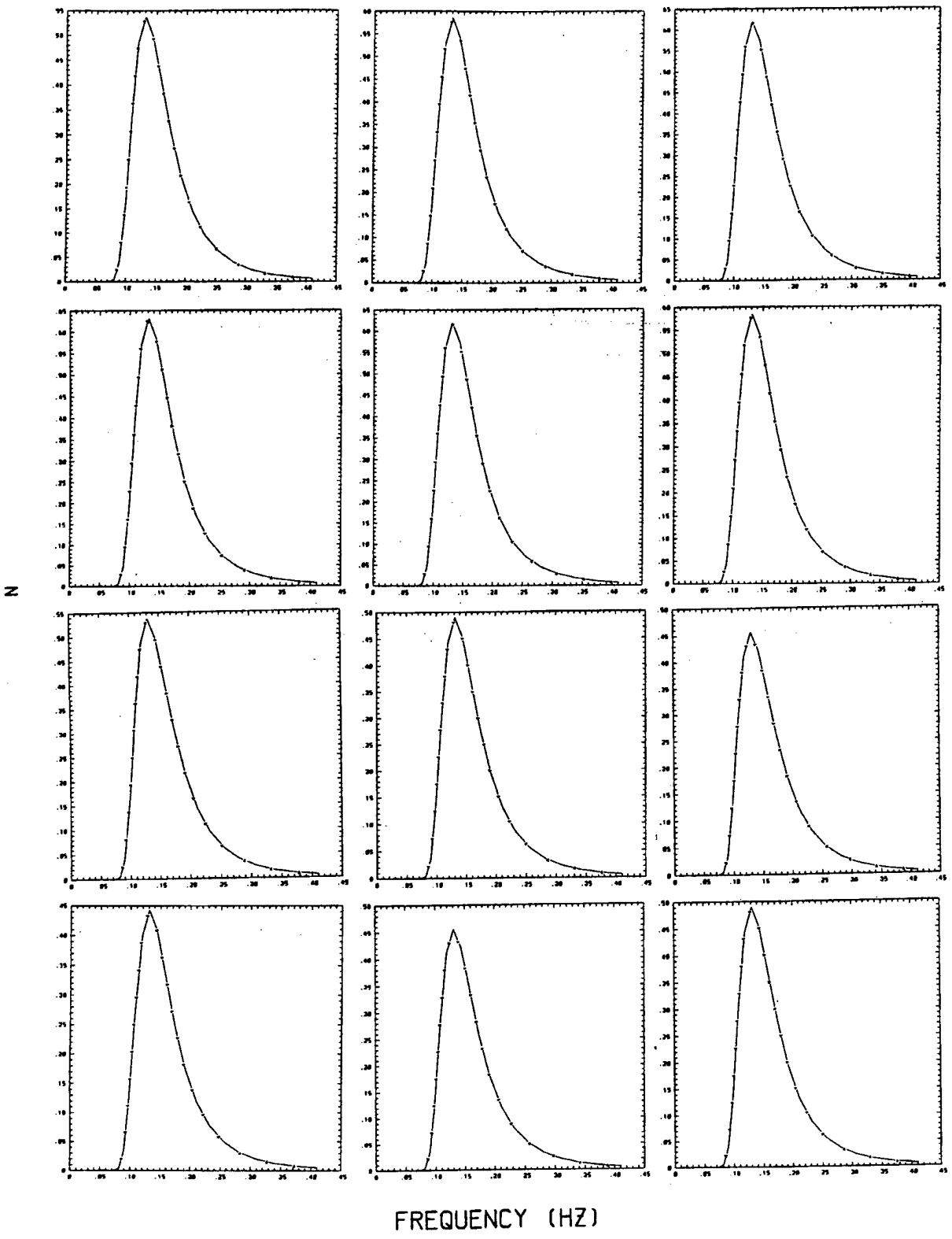

Fig. 4a. November energy density spectrum.

Fig. 4. is the same as Fig. 3, except that it shows maximum monthly mean during the past 30 years.

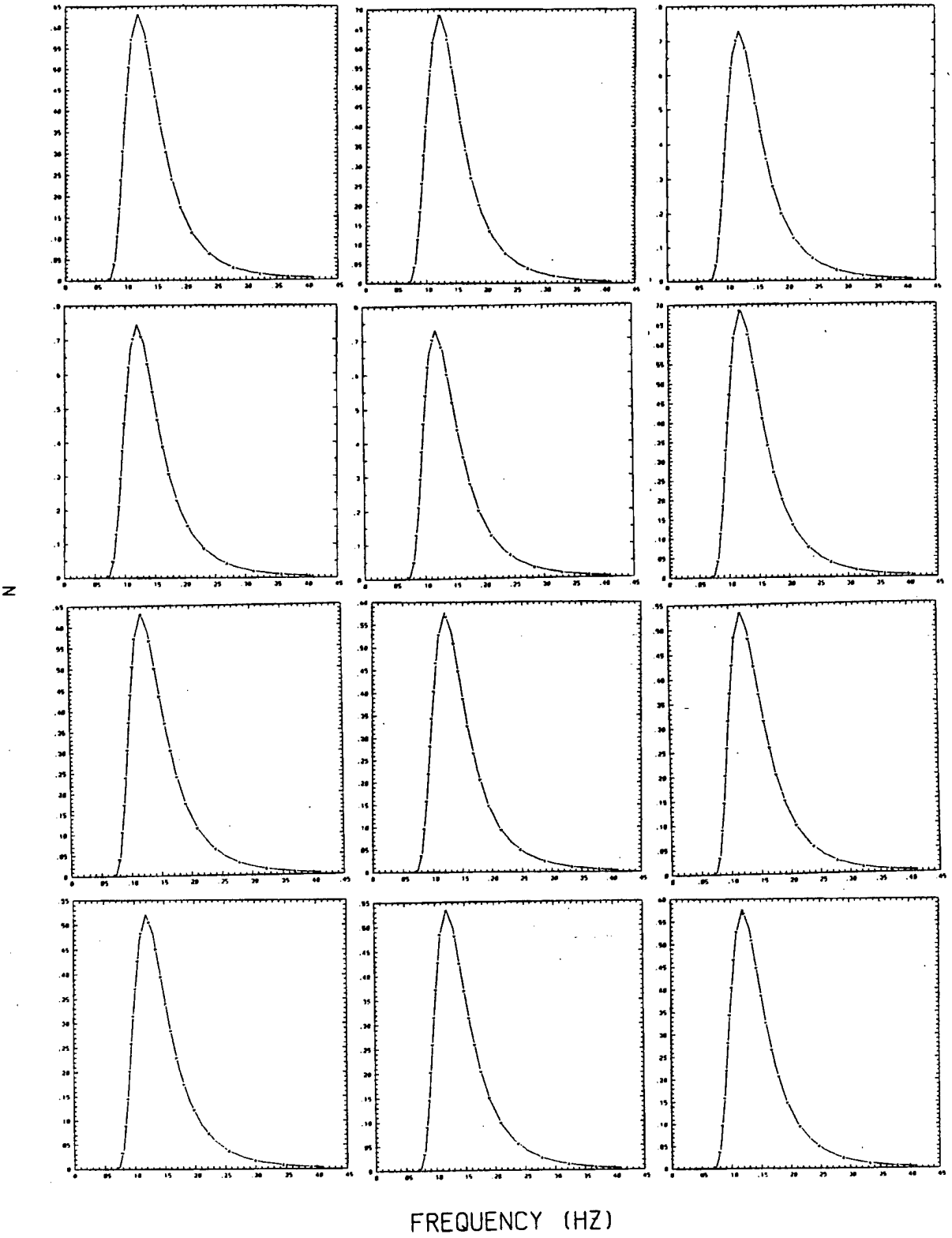

Fig. 4b. December energy density spectrum.

Fig. 4. (Continued)

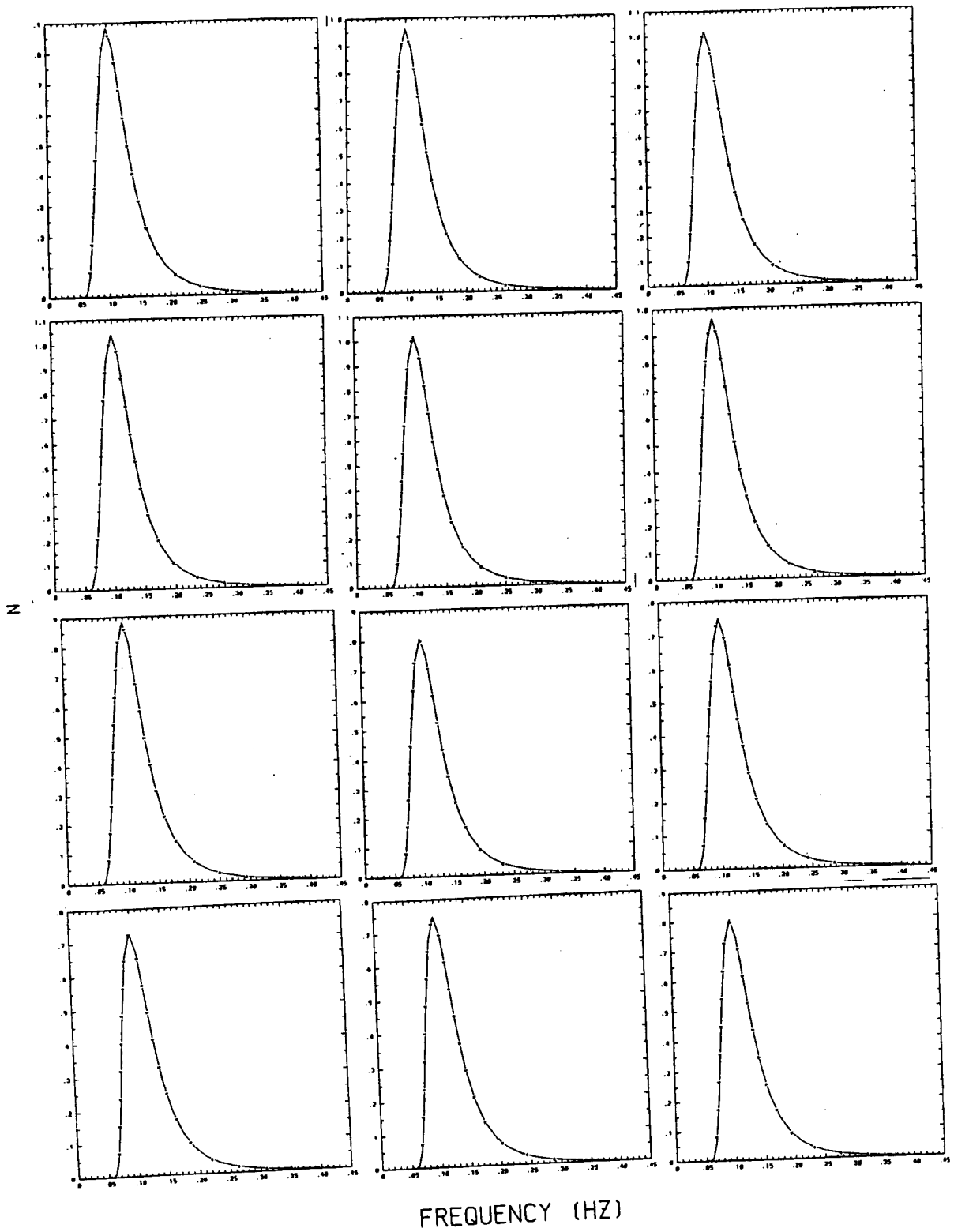

Fig. 4c. January energy density spectrum.

Fig. 4. (Continued)

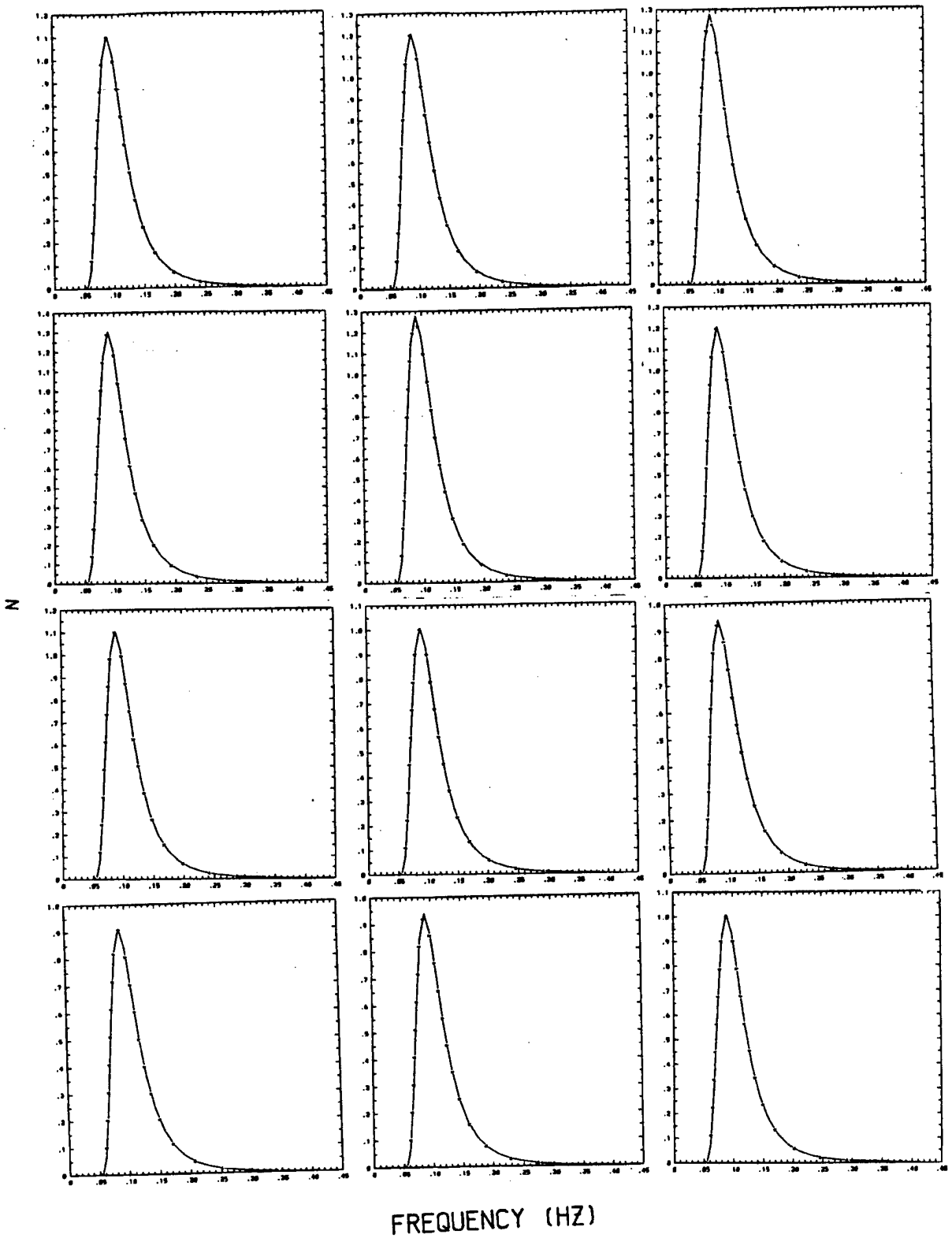

Fig. 4d. February energy density spectrum.

Fig. 4. (Continued)

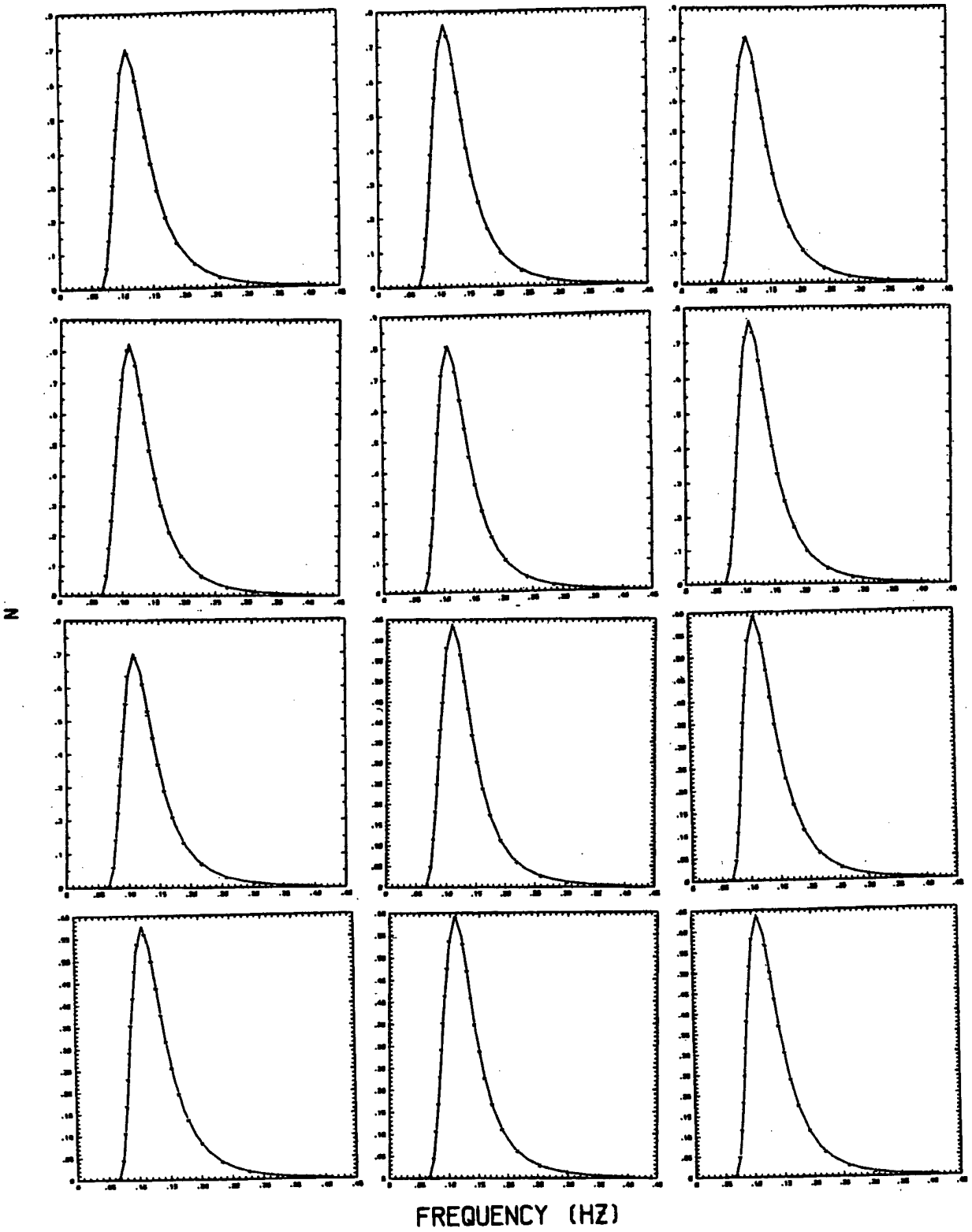

Fig. 4e March energy density spectrum.

Fig. 4. (Continued)

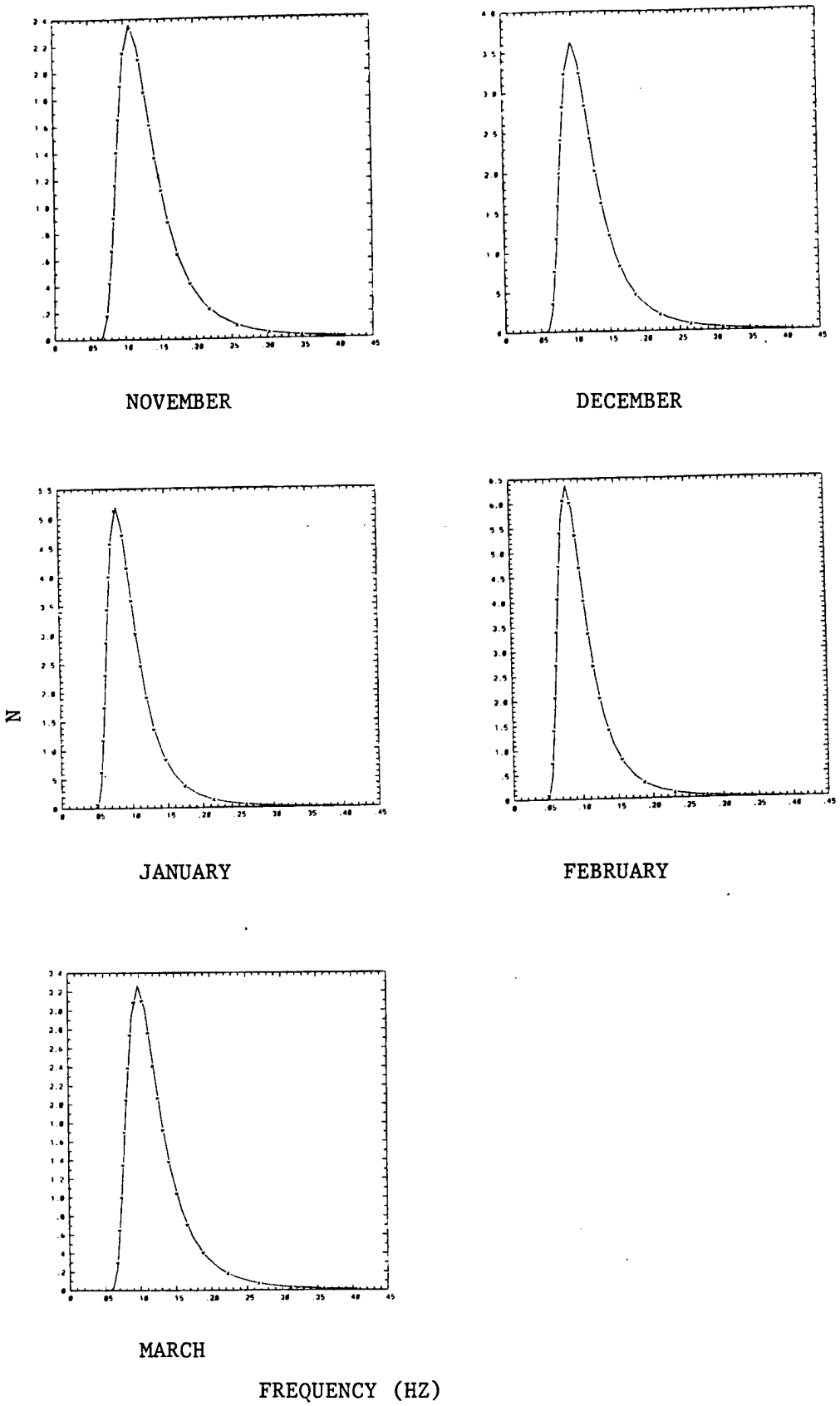

Fig. 5. One-dimensional spectrum in the extreme maximum case.

	Station	March	February	January	December	November
Mean	22N103E	12.72m/s	13.18m/s	11.74m/s	10.24m/s	10.50m/s
	12N106E	7.72m/s	13.02m/s	12.66m/s	9.80m/s	7.72m/s
	1N104E	3.27m/s	3.53m/s	3.50m/s	2.58m/s	2.17m/s
Max.	22N103E	20.03m/s	21.13m/s	17.27m/s	14.29m/s	13.80m/s
	12N106E	12.72m/s	20.88m/s	18.63m/s	13.67m/s	12.81m/s
	1N104E	5.15m/s	5.66m/s	5.15m/s	3.60m/s	3.60m/s
Gustin	Singapore	17.87m/s	23.17m/s	23.17m/s	20.59m/s	16.47m/s

Table 1. Monthly wind data (mean, maximum, extreme maximum) during the Northeast Monsoon season, was obtained from 30 years wind data at three stations: a). 22N, 103E; b). 12N, 106E; c). 1N, 104E.

Station	Mean	Maximum	Gusting
22N103E	10.75m/s	15.03m/s	
12N106E	7.78m/s	11.32m/s	
1N104E	3.25m/s	3.71m/s	16.51m/s

Table 2. Wind data (mean, maximum, extreme maximum) during December 11, 1985 to January 13, 1986 at three stations: a). 22N, 103E; b). 12N, 106E; c). 1N, 104E.

	Significant Wave Height (m)	Zero-crossing Wave Period (s)	Max. 3 hour Wave height (m)	Max. wave Height (m)	Maximum Period (s)
NCWM	4.72	8.73	9.02	7.79	10.24
WAM	3.54	7.61	6.77	5.84	9.23

Table 3a. Shows predicted waves from WAM and NCWM at 15N and 114E (water depth is greater than 1000 meters) during December 11, 1985-January 13, 1986, which is associated with Table 2.

		Significant Wave Height (m)	Zero-crossing Wave Period (s)	Max. 3 hour Wave height (m)	Max. wave Height (m)	Maximum Period (s)
Buoy	Max	0.88	6.7	1.77	1.69	9
	Average	0.41	3.78	0.82	0.64	5.17
NCWM	Max	0.91	6.8	1.78	1.62	9.11
	Average	0.43	3.81	0.83	0.71	5.21
WAM	Max	0.27	4.7	0.59	0.53	6.31
	Average	0.13	2.65	0.27	0.22	3.56

Table 3b. Shows predicted waves from WAM and NCWM at 1N and 104E (water depth is about 30 meters) during December 11, 1985-January 13, 1986, which is associated with Table 2.

		Significant Wave-height (m)	Zero-crossing wave period (sec)	Maximum Wave-height (m)	Peak Period (sec)	Max 3 hour wave-height (m)
March	Maximum	0.96	8.24	1.71	9.09	1.98
	Average	0.41	4.29	0.68	4.76	
February	Maximum	1.1	9.95	1.82	11.11	2.5
	Average	0.46	5.18	0.76	5.71	
January	Maximum	1.03	9.05	1.75	10.52	2.28
	Average	0.43	4.73	0.71	5.26	
December	Maximum	0.96	7.49	1.71	8.47	2.09
	Average	0.4	3.68	0.66	3.91	
November	Maximum	0.93	6.82	1.53	7.69	1.77
	Average	0.38	3.41	0.63	3.57	

Table 4. Singapore Harbor-Changi Airport Wave Climatology

INITIAL REPORT DISTRIBUTION

Number of Copies	NSWCCD Code	Name	Total Number of Copies
1	50	Morgan	1
1	50ff		2
1	5010	Raver	3
1	5060	506 (1 copy)	4
12	5500	Motter, Lin, Silver (10)	16
	ORGANIZATION	Name	
6	NFESC (East Det)	Seelig	22
1	NAVFAC	Curfman	23
1	ONR 321CD	Kinder	24
1	SEA 05HR	Pattison	25
2	DTIC	(2 copies)	27